

Van der Waals Spin-Orbit Torque Antiferromagnetic Memory

Lishu Zhang,^{1,*} Zhengping Yuan,^{2,*} Jie Yang,³ Jun Zhou,⁴ Yanyan Jiang,⁵
Hui Li,⁵ Yongqing Cai,⁶ Yuan Ping Feng,^{1,7,†} Zhifeng Zhu,^{2,‡} and Lei Shen^{8,§}

¹*Department of Physics, National University of Singapore, Singapore 117542, Singapore*

²*School of Information Science and Technology, ShanghaiTech University, Shanghai 201210, China*

³*Key Laboratory of Material Physics, School of Physics and Microelectronics,
Ministry of Education, Zhengzhou University, Zhengzhou 450001, China*

⁴*Institute of Materials Research & Engineering, A*STAR (Agency for Science,
Technology, and Research), Singapore 138634, Singapore*

⁵*Key Laboratory for Liquid-Solid Structural Evolution and Processing of Materials,
Ministry of Education, Shandong University, Jinan 250061, China*

⁶*Institute of Applied Physics and Materials Engineering,
University of Macau, Taipa, Macau SAR, China*

⁷*Center for Advanced 2D Materials, National University of Singapore, Singapore 117546, Singapore*

⁸*Department of Mechanical Engineering, National University of Singapore, Singapore 117542, Singapore*

The technique of conventional ferromagnet/heavy-metal spin-orbit torque (SOT) offers significant potential for enhancing the efficiency of magnetic memories. However, it faces fundamental physical limitations, including hunting effects from the metallic layer, broken symmetry for enabling anti-damping switching, spin scattering caused by interfacial defects, and sensitivity to stray magnetic fields. To address these issues, we here propose a van der Waals (vdW) field-free SOT antiferromagnetic memory using a vdW bilayer LaBr₂ (an antiferromagnet with perpendicular magnetic anisotropy) and a monolayer T_d phase WTe₂ (a Weyl semimetal with broken inversion symmetry). By systematically employing density functional theory in conjunction with non-equilibrium Green's function methods and macrospin simulations, we demonstrate that the proposed vdW SOT devices exhibit remarkably low critical current density approximately 10 MA/cm² and rapid field-free magnetization switching in 250 ps. This facilitates excellent write performance with extremely low energy consumption. Furthermore, the device shows a significantly low read error rate, as evidenced by a high tunnel magnetoresistance ratio of up to 4250%. The superior write and read performance originates from the unique strong on-site (insulating phase) and off-site (magnetic phase) Coulomb interactions in electrified LaBr₂, a large non-zero *z*-component polarization in WTe₂, and the proximity effect between them.

Introduction—A recent breakthrough in the field of current-induced spin-orbit torque (SOT) produced by ferromagnet/heavy-metal has provided a new and highly efficient method for magnetic state switching without an external magnetic field.[1, 2] However, there are several issues associated with this approach in conventional combination of metallic ferromagnets and bulk heavy metals, such as permalloy/Pt. Firstly, the critical current required for the switching process is relatively high.[3] Secondly, the switching speed is relatively slow.[1] Lastly, perpendicular magnetic anisotropy (PMA) MTJ, where the magnetization direction of the magnetic layers is oriented perpendicular to the plane, still necessitates a small in-plane magnetic field.[4, 5] Other critical issues for using 2D ferromagnetic materials include the low Currie temperature, for example 45 K of CrI₃,[6] and the hunting effects.[7]

Recently, Zhou et al., reported that monolayer LaBr₂ was a ferromagnetic electrified (in which excess electrons act as anions) with both large on-site and off-site Coulomb interactions.[8] The latter indicates a significant spatial charge fluctuation in LaBr₂. In 2022, bilayer LaBr₂ was reported to have interlayer antiferromagnetic property and perpendicular magnetic anisotropy.[9, 10] The large on-site Coulomb interaction leads to stronger

exchange interactions between the magnetic moments together with no stray fields in AFM LaBr₂, resulting in enhanced stability against thermal or external magnetic perturbations. Meanwhile, the large non-local Coulomb interaction provides a knob for effectively tuning the AFM spin, which is the key issue in conventional AFM spintronics. Thus, bilayer AFM LaBr₂ may be a good vdW magnetic material for SOT AFM memories. It is known that a small in-plane magnetic field is required for switching the magnetization of the PMA materials, which is another challenge for achieving ultralow power and miniaturized spintronic devices.[11] To realize field-free SOT MRAMs, low symmetric materials have been experimentally used for generating non-zero *z*-component spin polarization.[12] Very recently, Kajale et al., experimentally developed all-van der Waals (vdW) SOT devices with ferromagnetic Fe₃GaTe₂ and low symmetric T_d phase WTe₂ for deterministic switching of magnetization of Fe₃GaTe₃ in the absence of magnetic fields.[13]

In this study, we address the challenges in SOT ferromagnetic memories by utilizing 2D vdW antiferromagnetic system composed of bilayer LaBr₂ [9, 10] and monolayer T_d WTe₂. [14, 15] The reason we use T_d-phase WTe₂ as the SOT source for PMA LaBr₂ is that T_d-phase WTe₂ has a very small lattice mismatch with LaBr₂

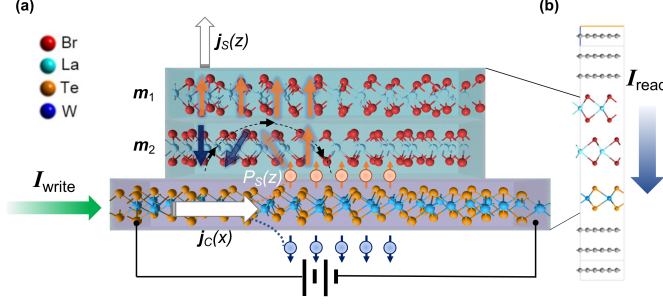


FIG. 1: Schematic view of the vdW LaBr₂/WTe₂ SOT antiferromagnetic memory, consisting of a perpendicular antiferromagnetic bilayer LaBr₂ and an asymmetric nonmagnetic metallic WTe₂. (a) **Write operation:** An in-plane electric current, injected parallel to the interface ($j_c(x)$), generates both an out-of-plane spin current ($j_s(z)$) and spin polarization ($P_s(z)$). The SOT switches the magnetization of the adjacent LaBr₂ layer (\mathbf{m}_2), while the magnetization \mathbf{m}_1 of the top layer remains unchanged. The green arrow indicates the memory writing current. (b) **Read operation:** The TMR effect in the vertical junction is employed to read the magnetic information in the bilayer LaBr₂. Two semi-infinite graphene leads facilitate the injection of the read current, indicated by a blue arrow.

(1.42 %). Furthermore, T_d-phase WTe₂ has broken inversion symmetry and substantial out-of-plane spin Hall conductivity (SHC) [15–17] which is anisotropic, providing a large polarization in the out-of-plane direction and field-free operation.[18–20] Our results show that this all-vdW field-free SOT antiferromagnetic random-access memory, integrating the write and read functions, has low power consumption through reduced switching current requirements, high-speed magnetic switching in picosecond, and a large tunnel magnetoresistance (TMR) for a low read error rate. Through both analytic analysis and macrospin simulations, we have observed an intrinsic critical current (I_c) of ~ 10 MA/cm² and a switching time (t) of ~ 250 ps in the bilayer LaBr₂/WTe₂ vdW structure. Regarding the read performance, we have discovered an exceptional tunnel magnetoresistance (TMR) value of 4250% employing non-equilibrium Green’s function (NEGF) calculations. The outperform write and read performance demonstrates the effectiveness and potential of our proposed 2D vdW AFM LaBr₂/WTe₂ system for SOT-MRAM applications.

Model—The atomic schematic diagram of the proposed vdW LaBr₂/WTe₂-based devices is shown in Fig. 1. The optimized interlayer distance is indicated in Fig. S1. In Fig. 1(a), when the write current is injected into the WTe₂ substrate, the spin current accumulates at the LaBr₂/WTe₂ interface and diffuses into the adjacent LaBr₂ layer. Consequently, spin-polarized electrons exert

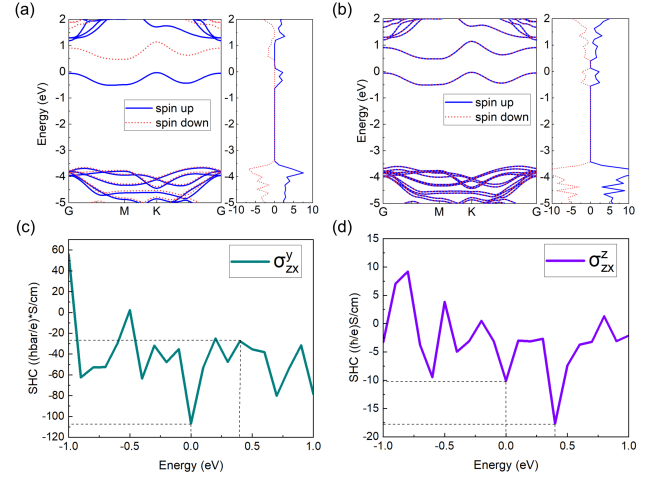


FIG. 2: The electronic structures of (a) the unit monolayer LaBr₂, and (b) the unit bilayer LaBr₂. (c-d) The variation of SHC with respect to the position of the Fermi energy for monolayer T_d WTe₂. The SHC tensor element σ_{zx}^y , is not equal to zero because of the broken symmetry in T_d WTe₂. The Fermi energy is set to zero, at which $\sigma_{zx}^y = -106$ (h/e)²S/cm, $\sigma_{zx}^z = -10.5$ (h/e)S/cm, and the ratio of σ_{zx}^z to σ_{zx}^y , defined as $\tan\beta$, is 0.10. The ratio will significantly increase to 0.65 when the Fermi level is shifted up to 0.4 eV by electric fields, providing a large out-of-plane spin-polarized current and field-free switching of magnetization of the adjacent LaBr₂ layer.

a torque on the local magnetic moment by transferring their angular momentum, facilitating the switching of the magnetization \mathbf{m}_2 of the LaBr₂ layer adjoining the WTe₂ layer (as illustrated in Fig. S2). The T_d-phase of WTe₂, belonging to the space group Pmn2₁, exhibits strong SHC and high spin Hall angles (SHA). The band structure of *monolayer* LaBr₂ is presented in Fig. 2(a). The presence of two localized states near the Fermi level corresponds to the spatial electric states, with one state fully occupied and the other fully empty. Figure 2b shows the *bilayer* LaBr₂ which exhibits antiferromagnetic behavior. Further SOC calculations indicate the out-of-plane spin polarization in bilayer LaBr₂ (\mathbf{m}_1 and \mathbf{m}_2 in Fig. 1). Two components of the spin Hall conductivity (σ_{zx}^y and σ_{zx}^z) of T_d-phase WTe₂ are shown in Fig. 2(c-d). Notably, the σ_{zx}^z is one order of magnitude smaller than σ_{zx}^y at the Fermi level, while the value of σ_{zx}^z is significant at 0.4 eV below E_f and even comparable to the σ_{zx}^y . This large z-component SHC is in agreement with the experimental value reported for other Weyl semimetals [21]. In the late part, using macrospin simulation we will demonstrate how such large ratio of σ_{zx}^z over σ_{zx}^y can effectively and quickly switch magnetization of \mathbf{m}_2 layer of LaBr₂ with only small charge current.

Write—To gain insights into the magnetization dynamics of LaBr₂, we conducted numerical simulations using the two-sublattice macrospin model (see METHODS for more details), applying a charge current (\mathbf{J}_{SOT})

TABLE I: The DFT and experimental parameters for macromagnetic simulations.

Parameter	Symbol	Value	Remark
Magnetic moment per unit cell	μ	$1 \mu\text{B}$	
Volume of unit cell	V	$8.26 \times 10^{-29} \text{ m}^3$	
Saturation magnetization	M_S	112 emu/cm^3	
Magnetic anisotropy energy	EMA	0.27 meV	Out-of-plane
Interlayer exchange	J_{12}	0.132 meV	
Intralayer exchange	J_{13}	6.38 meV	AFM
Magnetic anisotropy constant	K_u	$5.24 \times 10^5 \text{ J m}^{-3}$	
Anisotropic field	H_k	9.33 T	
Exchange field	H_{ex}	2.27 T	
Damping constant	σ	0.015	[22]
Spin Hall angle	θ_{SH}	0.323	[14, 15]
Spin Hall conductivity (y -polarization)	σ_{zx}^y	-18	At $E_f = -0.4 \text{ eV}$
Spin Hall conductivity (z -polarization)	σ_{zx}^z	-16	At $E_f = -0.4 \text{ eV}$
Conductivity angle	$\tan \beta$	0.89	$(\sigma_{zx}^z)/(\sigma_{zx}^y)$

along the x -direction to the heavy metal (HM) layer. The device structure is shown in Fig. 1, where \mathbf{m}_1 denotes the magnetic moment of the upper LaBr₂ layer and \mathbf{m}_2 represents the magnetic moment of the lower layer LaBr₂. Meanwhile, the parameters used in the macrospin simulation are summarized in Table I, where the spin polarization $\sigma = (0, \cos \beta, -\sin \beta)$. The dynamics of the bilayer LaBr₂/WTe₂ heterojunction with different spin- z components corresponds to varying β . Specifically, we chose $\beta = 60^\circ$, corresponding to WTe₂ with $E - E_f = 0.4 \text{ eV}$, to investigate the switching properties of \mathbf{m}_1 and \mathbf{m}_2 . The switching paths of the two magnetic moments are shown in Fig. 3(a). Driven by damping-like torque (DLT), the magnetic moment \mathbf{m}_2 undergoes a switching process from the $-z$ direction to the $+z$ direction, while the magnetic moment \mathbf{m}_1 remains in the $-y$ direction. Consequently, \mathbf{m}_1 and \mathbf{m}_2 transition from an antiparallel (AP) state to a parallel (P) state, resulting in the conversion of the system from an AFM mode to an FM mode. Meanwhile, the switching of \mathbf{m}_2 is deterministic and stable. It should be noted that this switching process does not necessitate an external magnetic field and can be accomplished through the application of a DC current, eliminating the need for a two-step process of conventional SOT-driven switching. In addition, the switching process is within 250 ps, as shown in Fig. 3(b), which is much shorter than the traditional three-terminal FM device driven by SOT.

In order to further reveal the impact of z -direction spin polarization on SOT switching efficiency, the relationship between switching time (t_{sw}) and applied current density \mathbf{J}_{SOT} under different β in the case of only DLT is investigated. Here, t_{sw} is defined as the time required for the magnetic moment \mathbf{m}_2 to proceed from the initial position $(0, 0, -1)$ to $\mathbf{m}_{2,z} = 0.9$ [23]. As shown in Fig. 3(c), increasing the current density speeds up the switching process for all β values. Additionally, Under the same current density, the t_{sw} corresponding to dif-

ferent β is significantly different, and a large angle corresponds to faster switching. Furthermore, the impact of field-like torque (FLT) on the system and the coexistence of DLT and FLT are also studied. Similar to the case with only DLT, the magnetic moment \mathbf{m}_2 undergoes switching, and the presence of FLT affects the precession process. Comparing Fig.3(b) and Fig. S2(c), it is demonstrated that when the value of FLT is large ($\eta_{FLT} = 4$), its influence on the precession process becomes more pronounced, resulting in a further reduction in the time required for \mathbf{m}_2 switching and a significant decrease in the oscillation amplitude of m_1 along the z direction. The presence of FLT facilitates the switching of the magnetic moment \mathbf{m}_2 . On the other hand, Fig. 3(d) reveals that with only FLT, the magnetic moment \mathbf{m}_1 experiences minimal movement, while \mathbf{m}_2 exhibits slight oscillations along the $-z$ direction, even at a high current density ($\mathbf{J}_{\text{SOT}} = 100 \text{ MA/cm}^2$). This indicates that the switching process of 2D LaBr₂ with in-plane anisotropy and spin- z is predominantly governed by DLT, and the presence of FLT influences the precession process. Additionally, we studied the relationship between t_{sw} and \mathbf{J}_{SOT} under different β under the coexistence of DLT and FLT. As shown in Fig. 3(d), similar to the case of only DLT, the change of β has a significant impact on t_{sw} , but it is not as severe as the case of only DLT. At the same time, under the same β and \mathbf{J}_{SOT} , the system where DLT and FLT coexist switches faster, which further proves that FLT promotes switching.

Fig. 3(e) shows the relationship between critical current density (\mathbf{J}_c) corresponding to different β measured through simulation. For the two cases where only DLT or DLT is accompanied by FLT, the critical current density decreases significantly with the increase of the presence of a significant out-of-plane SHC, and tends to be stable at larger angles. Conversely, if the material lacks out-of-plane SHC, a significantly higher \mathbf{J}_c would be required. This further emphasizes the significance of selecting T_d -

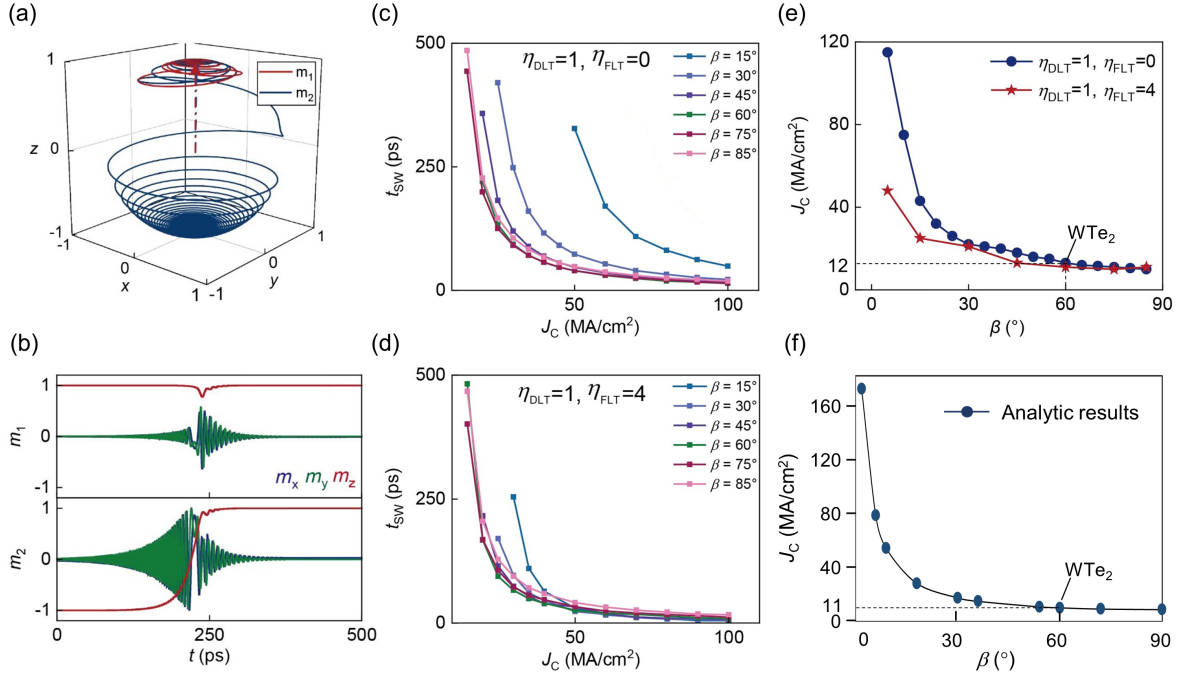


FIG. 3: The time evolution of (a) the trajectories of magnetic moments and (b) the components of \mathbf{m} in the x , y , and z directions. The switching time as a function of applied current density at different spin polarization directions with (c) $\eta_{DLT} = 1$ and $\eta_{FLT} = 0$ and (d) $\eta_{DLT} = 1$ and $\eta_{FLT} = 4$. (e) The critical current density as a function of β . (f) The analytical critical current density is a function of varying β when the FLT is zero.

phase WTe₂ for our study, rather than other highly symmetric SOC materials.[12] Moreover, for the case where DLT and FLT coexist, with the same β , the critical current density is lower than in the case of only DLT. The analytic results of the relationship between \mathbf{J}_c and β are shown in Fig. 3(f), which demonstrates the similarity between numerical simulation and analytic results. A critical current of 12 MA/cm² for WTe₂ in Fig. 3(e) is similar to 11 MA/cm² in Fig. 3(f).

Read—Apart from the aforementioned write operation, the read process, which relies on the TMR effect, serves as another crucial function in magnetic memories. To investigate the TMR effect of our vdW LaBr₂/WTe₂ heterojunction, a vertical model is constructed as shown in Fig. 1(b). In this model, the P or AP state is defined as the parallel (antiparallel) magnetic orientation between two LaBr₂ layers (Fig. 1(a)). The lower LaBr₂ layer serves as the free layer, while the upper LaBr₂ layer acts as the pinning layer. A vertical current is injected between semi-infinite graphite leads, sandwiching the LaBr₂/WTe₂ structure.

The TMR of the such vertical MTJ at the equilibrium state (zero bias voltage) is first calculated. At the equilibrium state, the TMR is defined as $TMR = (T_P - T_{AP})/T_{AP} \times 100\%$, where $T_{P(AP)}$ represents the transmission coefficient at the Fermi level for the P and AP state, respectively. A large TMR of 4250% is obtained. This is due to the transmission coefficient of the

P state being over an order of magnitude larger than that of the AP state. A relatively larger T_P and a smaller T_{AP} contribute to a considerable TMR. To understand the origin of this high TMR effect, the k_{\parallel} -resolved transmission spectra are plotted in Fig. S3. The conductance is the integration of transmission over all k_{\parallel} points in the 2D Brillouin zone. In the spin up of the P state, stronger peaks with $T_{PC\uparrow} = 0.16$ at the Γ point results in the high conductance of the P state.

Under the nonequilibrium state or bias, Fig. 4(a-b) show the I-V curves for the spin up and spin down states in both the P and AP states. It can be seen that the current in the P state is an order of magnitude larger than that in the AP state, indicating good TMR performance. The current in the spin down channel for the P state is unchanged in an "off" state, as shown in Fig. 4(a). In contrast, for the AP magnetic state, the current in the spin down channel generally increases with the bias voltage. Moreover, both the spin up and spin down currents exhibit an "on" state, which is different from the behavior observed in the P magnetic state. The calculated TMR is shown in Fig. 4(c), which is defined as $TMR = \frac{I_P - I_{AP}}{I_{AP}} \times 100\%$. Here, I_P and I_{AP} represent the currents for the P and AP magnetic states, respectively. Notably, TMR is inversely proportional to the current for the AP state. Therefore, as the bias increases or decreases, the TMR decreases due to the enhancement of current for the AP state. Fig. 4(d) shows the

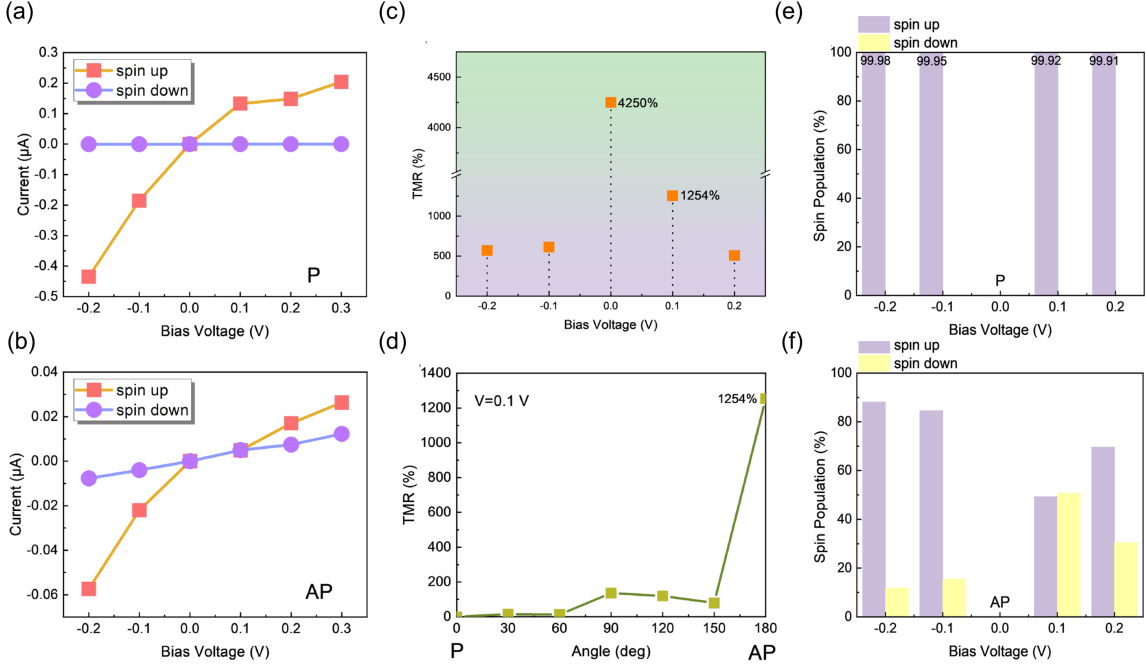


FIG. 4: The spin-resolved current of spin up and spin down for (a) P and (b) AP states. (c) Bias dependence of TMR ratio and (d) Angle θ , between two magnetizations on two monolayers of LaBr₂, dependence of non-collinear TMR with fixed bias of 0.1V. Spin polarization of (e) the P state and (f) AP state.

angle dependence of TMR under 0.1 V bias, which is defined as $TMR(\theta) = \frac{I(\theta) - I(0)}{I(0)}$, where $I(0)$ represents the current for the P state with the magnetization of the bilayer LaBr₂ aligned in parallel, and $I(\theta)$ represents the current for a polar angle θ between two magnetization directions, and $I(\theta = 180^\circ)$ corresponds to the AP state. It is found that during the switching process from the P state ($\theta = 0^\circ$) to the AP state ($\theta = 180^\circ$), the TMR gradually increases and finally reaches the maximum value. Besides TMR, the spin population, denoted as $SP\alpha = \frac{I\sigma}{I_{Total}} \times 100\%$ ($\sigma = \text{up, down}$), is calculated, as illustrated in Fig.4(e-f). The results clearly demonstrate that, in comparison to the AP state, the spin population of the P state can achieve and sustain nearly 100%, indicating an ideal spin-filtering characteristic that selectively permits the passage of spin-up current only, which is supported by the transmission spectra (Fig. S5).

In Fig. 4(a-b), we note that the spin down current is not zero in the AP configuration, leading to low spin polarization. This problem can be addressed by constructing a double spin-filter tunnel junction[24], inserting an insulating monolayer *h*-BN between the bilayer LaBr₂. Unlike conventional MTJs, the two insulating magnetic LaBr₂ selectively filter one of the two electron spin directions [25], resulting in perfect spin polarization under positive bias as shown in Fig. S6(b-c). We also calculate the rectification ratios of the vdW LaBr₂/LaBr₂/WTe₂ and LaBr₂/BN/LaBr₂/WTe₂ MTJs under different bias voltages (Table S1). A clear comparison reveals that the

inclusion of *h*-BN leads to improved rectification ratios, reaching up to 78.56 %.

In conclusion, we have designed all-van der Waals AFM-LaBr₂/WTe₂ heterostructures with exceptional data write and read capabilities. Compared to devices made of 3D ferromagnetic materials, our two-sublattice macrospin simulations show that the use of 2D material LaBr₂ allows for faster switching at comparable or even lower current densities. The remarkable out-of-plane spin Hall conductivity of WTe₂ and delocalized nature of electride LaBr₂ enable such fast and efficient spin-orbit torque switching of magnetization. Additionally, a high TMR ratio of up to 4250% and a high spin polarization of close to 100% in the proposed system are achieved. The underlying microscopic physics responsible for this intriguing read performance have been analyzed through the examination of transmission spectra. The excellent performance highlights the tremendous potential of vdW PMA AFM LaBr₂ in advancing spintronic device applications. Specifically, it opens avenues for the design of ultra-low power, ultra-fast data operation, ultra-high density, and thermally stable memories.

ACKNOWLEDGEMENT

The authors thank the support from the National Natural Science Foundation of China (Grant No.12104301, No. 51671114 and No. U1806219), MOE Singapore

(MOE2019-T2-2-030, A-0005241-01-00 and A-8001194-00-00). This work is also supported by the Special Funding in the Project of the Taishan Scholar Construction Engineering.

* These authors contributed equally to this work.

† phyfyp@nus.edu.sg

‡ zhuzhf@shanghaitech.edu.cn

§ shenlei@nus.edu.sg

- [1] V. Krizakova, M. Perumkunnil, S. Couet, P. Gambardella, and K. Garello, *Journal of Magnetism and Magnetic Materials* **562**, 169692 (2022).
- [2] D. Wang, Z. Wang, N. Xu, L. Liu, H. Lin, X. Zhao, S. Jiang, W. Lin, N. Gao, M. Liu, *et al.*, *Advanced Science* **9**, 2203006 (2022).
- [3] W. Kong, C. Wan, C. Guo, C. Fang, B. Tao, X. Wang, and X. Han, *Applied Physics Letters* **116**, 162401 (2020).
- [4] P. Shukla, P. Kumar, and P. K. Misra, *IEEE Transactions on Magnetics* **58**, 1 (2022).
- [5] K. Zhang, K. Cao, Y. Zhang, Z. Huang, W. Cai, J. Wang, J. Nan, G. Wang, Z. Zheng, L. Chen, *et al.*, *IEEE Electron Device Letters* **41**, 928 (2020).
- [6] B. Huang, G. Clark, D. R. Klein, D. MacNeill, E. Navarro-Moratalla, K. L. Seyler, N. Wilson, M. A. McGuire, D. H. Cobden, D. Xiao, *et al.*, *Nature nanotechnology* **13**, 544 (2018).
- [7] M. Wang, J. Zhou, X. Xu, T. Zhang, Z. Zhu, Z. Guo, Y. Deng, M. Yang, K. Meng, B. He, *et al.*, *Nature Communications* **14**, 2871 (2023).
- [8] J. Zhou, Y. P. Feng, L. Shen, *et al.*, *Physical Review B* **102**, 180407 (2020).
- [9] Q. Chen, X. Zheng, P. Jiang, Y.-H. Zhou, L. Zhang, and Z. Zeng, *Physical Review B* **106**, 245423 (2022).
- [10] W. Sun, W. Wang, H. Li, X. Li, Z. Yu, Y. Bai, G. Zhang, and Z. Cheng, *npj Computational Materials* **8**, 159 (2022).
- [11] R. Sbiaa, H. Meng, and S. Piramanayagam, *physica status solidi (RRL)–Rapid Research Letters* **5**, 413 (2011).
- [12] K. Dolui, M. D. Petrovic, K. Zollner, P. Plechac, J. Fabian, and B. K. Nikolic, *Nano letters* **20**, 2288 (2020).
- [13] S. N. Kajale, T. Nyugen, M. Li, and D. Sarkar, *arXiv preprint arXiv:2309.04930* (2023).
- [14] K. Kang, T. Li, E. Sohn, J. Shan, and K. F. Mak, *Nature materials* **18**, 324 (2019).
- [15] J. Zhou, J. Qiao, A. Bournel, and W. Zhao, *Physical Review B* **99**, 060408 (2019).
- [16] S. Wu, V. Fatemi, Q. D. Gibson, K. Watanabe, T. Taniguchi, R. J. Cava, and P. Jarillo-Herrero, *Science* **359**, 76 (2018).
- [17] S. Tang, C. Zhang, D. Wong, Z. Pedramrazi, H.-Z. Tsai, C. Jia, B. Moritz, M. Claassen, H. Ryu, S. Kahn, *et al.*, *Nature Physics* **13**, 683 (2017).
- [18] A. van den Brink, G. Vermeij, A. Solignac, J. Koo, J. T. Kohlhepp, H. J. Swagten, and B. Koopmans, *Nature communications* **7**, 10854 (2016).
- [19] Y. Song, Z. Dai, L. Liu, J. Wu, T. Li, X. Zhao, W. Liu, and Z. Zhang, *Advanced Electronic Materials* **9**, 2200987 (2023).
- [20] Y. Liu, B. Zhou, and J.-G. Zhu, *Scientific reports* **9**, 325 (2019).
- [21] B. Zhao, D. Khokhriakov, Y. Zhang, H. Fu, B. Karpiak, A. M. Hoque, X. Xu, Y. Jiang, B. Yan, and S. P. Dash, *Physical Review Research* **2**, 013286 (2020).
- [22] D. M. Lattery, D. Zhang, J. Zhu, X. Hang, J.-P. Wang, and X. Wang, *Scientific reports* **8**, 1 (2018).
- [23] Y.-J. Tsou, W.-J. Chen, H.-C. Shih, P.-C. Liu, C. Liu, K.-S. Li, J.-M. Shieh, Y.-S. Yen, C.-H. Lai, J.-H. Wei, *et al.*, *IEEE Transactions on Electron Devices* **68**, 6623 (2021).
- [24] G.-X. Miao, M. Müller, and J. S. Moodera, *Physical review letters* **102**, 076601 (2009).
- [25] J. S. Moodera, T. S. Santos, and T. Nagahama, *Journal of Physics: Condensed Matter* **19**, 165202 (2007).